Xin He, Qiang Li, Valentin L. Popov

Strength of adhesive contact between a rough fibrillar structure and an elastic body: influence of fibrillar stiffness

Strength of adhesive contact between a rough fibrillar structure and an elastic body: Influence of fibrillar stiffness

Xin He[a], Qiang Li[a] and Valentin L. Popov[a,b]*

[a]*Institute of Mechanics, Berlin University of Technology, Berlin, Germany;* [b]*National Research Tomsk State University, Tomsk, Russia*

X. He: hexin2009@hotmail.com

Q. Li: qiang.li@tu-berlin.de

V. L. Popov: v.popov@tu-berlin.de

Strength of adhesive contact between a rough fibrillar structure and an elastic body: Influence of fibrillar stiffness

Adhesive contact between a rough fibrillar structure and an elastic half space is numerically studied using the boundary element method. The fibrils are modelled as soft cylinders with constant stiffness and a gaussian distribution of heights. Adhesive strength is obtained as function of preload, roughness, and fibril stiffness. The adhesive strength after large enough preloading increases with decrease of fibril stiffness tending to a limiting value, which is independent of roughness. The present model aims to bridge the limiting cases of very rigid fibrils and extremely soft fibrils. In particular, we determined the stiffness needed to make the adhesion stress "tolerant" to the roughness, and an enhancement of adhesion is obtained by decreasing stiffness.

Keywords: adhesion; rough contact; simulation; fibrillar stiffness; Boundary Element Method

1 Introduction

Adhesive contact of rough surfaces has been very intensively investigated in the last few decades. One of the hot topics were fibrillar structures, which are found in many bio-systems, e.g., feet of geckos [1]-[3], which contains millions of array-like forms of microcosmic fibrils with hierarchical structures (branch-seta-spatula), and this is regarded as the main contributing factor to its strong adhesion ability. There is a large number of studies seeking for understanding of the mechanism of strong attachment of these structures, starting with the simple idea contact splitting to complicated hierarchical structures, mimicking the biological attachment systems [4]-[9]. Hui et al. proposed a splitting model containing an independent array of springs with spherical tips, and the length of fibrils was ruled by Gaussian distribution to represent the height of the surface asperities [5][6]. The compensation through increasing the compliance of fibrils can weaken the detrimental effect of roughness. Schargott proposed a hierarchical model based on the tokay gecko's pad, to investigate the adhesive contact with a rough surface

[9]. By increasing number of hierarchical layers which essentially increases the compliance of the system, a stronger adhesive force was obtained.

The basis for analysis of complicated structures remains the adhesin theory by Johnson, Kendall and Roberts (JKR) [10] or for simple cylindrical fibrils the Kendall's solution [11][12][13]. Based on the theoretical studies, technologies for fabrication of structured surfaces mimicking the function of gecko's feet have been developed. Micropillar-patterned PDMS surfaces have shown a stronger adhesion compared with unpatterned surfaces [14]. It was found that elastic fibrils possess better adaptability to comply surfaces, even to rough surfaces [15]. Surfaces with artificial geometry such as concave shape could optimize the stress distribution and then enhance adhesive strength [16]. For structural applications, Heide-Jørgensen et al. investigated an array-structure of pillars in the double cantilever beam (DCB) theoretically and experimentally, and altered the geometry of pillars to affect the fracture behaviour of the DCB and then increase the toughness of the material [17]. Morano et al. suggested an introduction of channel in the sub-surface of an interface, which can affect the dissipated energy through channel geometry [18]. Since 2000s, the concept of contact splitting became popular for explanation of strong adhesive strength of fibrillar interfaces which states that splitting of a large, compact surface into smaller discrete sub-surfaces leads to an increase of adhesive force [19][20]. It can be attributed to the fact that the adhesive strength turns larger as the size of fibrils decreases, since a higher critical stress is needed for the separation of a single fibril; on the other side, splitting the surface could optimize the stress concentration at the edge of contact and obtain a much uniform stress distribution. Takahashi numerically studied a multi-spring model based on the FEM [21]. The multi-spring model is governed by the JKR theory and each spring acts individually. Bhushan assembled springs to a hierarchical model based on force balance [22]. The DMT theory is applied to each spring in the bottom-layer, and higher adhesion is observed. While a recent numerical study on flat-ended brush structures showed, however, that the contact splitting alone does not increase the adhesive strength. On the contrary, if the “splitted spots” are connected rigidly with each other, this always leads to a decrease of the adhesive strength (approximately proportional to the “filling factor” of microcontacts compared with the whole apparent contact area [23]). But if the fibrils possess elasticity, the adhesive strength can increase or decrease - depending on the number and elasticity of the fibrils [24]. In the present work, we consider the rough contact with a gaussian height distribution. We use the mesh-dependent detachment criterion which previously has been shown to be equivalent to the JKR theory. The elastic coupling of fibrils is treated numerically exactly, without any further simplifications.

Adhesive contact between the rough pillar structure and an elastic half space is numerically simulated using the Fast Fourier Transform-assisted Boundary Element Method (FFT-assisted BEM) [25][26]. The fibrils are modelled as elastic cylinders while the counter-partner as elastic half space. The numerical procedure is described in the previous paper [24]. The rough brush-structure with rigid pillars was studied in ref [27]. In this paper we focus on the influence of fibril stiffness.

2 Numerical model and simulation method

The numerical model is shown in Figure 1. The elastic half space has the elastic modulus E and Poisson’s ratio ν. The brush structure is composed of a large number of cylindrical pillars with the same radius. The lengths of pillars, are, however, characterized by the probability density function

$$\Phi(l) = \frac{1}{\sqrt{2\pi\sigma}} \mathrm{e}^{-\frac{(l-l_0)^2}{2\sigma^2}}, \tag{1}$$

where l is the height of pillars, σ and l_0 are the standard deviation and the mean value respectively. The parameter σ describes the characteristic roughness of the fibrillar structure. The elasticity of the pillars is modelled by the rigid cylinders coupled elastically to a rigid plate with linear springs as shown in Figure 1, which is equivalent to a system with a thin elastic layer between cylinders and a rigid plate [29] (Figure 1 right).

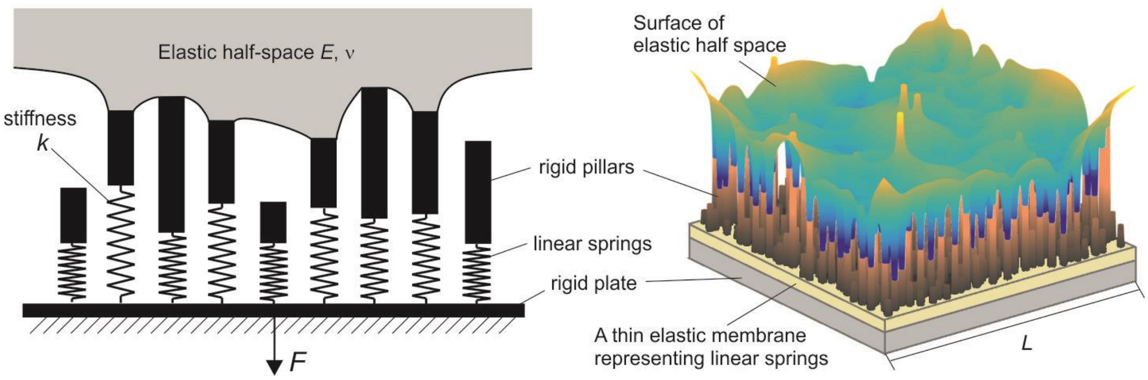

Figure 1 Sketch of adhesive contact between a elastic rough fibrillar structure and an elastic half space. The right figure shows a three-dimensional illustration.

Under the normal load on the rigid plate, the fibrillar structure is pressed into the elastic half space by an indentation depth d. Effects of buckling are not considered in the present work. For the elements in contact, this macroscopic indentation depth (displacement of the structure) contains two parts: the surface displacement of elastic half-space u and the displacement of the corresponding spring Δl (or elongation of the fibrils, see Figure 1). Therefore, the following condition is satisfied:

$$d = u + \Delta l. \tag{2}$$

We assume that all springs have the same normal stiffness k. The equilibrium condition for the contact of the n-th pillar with the elastic half space reads

$$f_n = k\Delta l_n = \int_{A_n} p_n \mathrm{d}A_n \,, \tag{3}$$

where p_n is the pressure distribution in the contact of the pillar with the half-space, A_n is the contact area of the pillar. Substitution of (3) into (2) gives

$$u_n = d - \frac{1}{k}\int_{A_n} p_n \mathrm{d}A_n\,. \tag{4}$$

Here u_n is the surface displacement of elastic half space in the area of A_n. It is noted that it is generated not only from the pressure p_n in this area of A_n but from the pressure in the whole contact region.

The normal displacement of elastic half space $u(x,y)$ under the action of normal stress distribution $p(x',y')$, is described by integration of the fundamental solution of Boussinesq [28],

$$u_{\mathrm{z}}(x,y) = \frac{1}{\pi E^*}\int_X\int_Y \frac{1}{\sqrt{(x-x')^2+(y-y')^2}}\, p(x',y')\mathrm{d}x'\mathrm{d}y'. \tag{5}$$

In a discrete form, it can be written as

$$u_{ij} = K_{iji'j'}p_{i'j'}, \tag{6}$$

where u is the displacement of surface element at position (i, j) in two-dimensional discretization, p is the normal stress acting on the element (i',j'), K is the influence coefficient. We discretize the simulation area in square elements with the total number of $N\times N$; the stress p and the displacement u have the same matrix dimension $N\times N$, and the matrix K of influence coefficients has the dimension of $N^2\times N^2$. To reduce the complexity, the Fast Fourier Transform (FFT) is usually applied to accelerate the computation of the convolution (6), which reduces the complexity from $o(N^4)$ to $o(N^2\log N^2)$ [30]. Before carrying out the FFT, the matrix of influence coefficient is usually constructed in the 'convolution' form of having the same dimension $N\times N$:

$$u = K * p, \tag{7}$$

where "*" means convolution operation. The operation of FFT is then

$$u = \mathrm{IFFT}[\mathrm{FFT}(K)\cdot\mathrm{FFT}(p)]. \tag{8}$$

In a recent study on flat-ended soft brush structure [24] the BEM was further developed to take into account of pillar stiffness directly. The relation between the macroscopic indentation depth and pressure distribution on elastic half space is obtained by

$$d = \frac{h^2}{k}\Pi * p + K * p = \left[\frac{h^2}{k}\Pi + K\right] * p, \tag{9}$$

where Π is a new matrix of influence coefficient whose elements are equal either one or zero and its distribution in matrix depends on the size of pillars. The first term in Eq. (9) is actually the displacement of springs but in a "convolution" form. Eq. (9) considers the displacement of both springs and the elastic half-space simultaneously. Similarly, the FFT can be carried out for Eq. (9)

$$d = \mathrm{IFFT}\left[\mathrm{FFT}\left(\frac{h^2}{k}\Pi + K\right) \cdot \mathrm{FFT}(p)\right]. \tag{10}$$

In this way, the spring stiffness is directly integrated into the influence matrix. The details on this method can be found in [24].

In numerical simulation, we give the general displacement of the fibrillar structure d (displacement-controlled indentation). The stress p can be obtained by solving the Eq. (10) using the conjugate-gradient method [25], then the displacement of the elastic half-space u can be determined by Eq. (8) based on the balanced stress distribution p, and the displacement of springs Δl is obtained from Eq. (2) based on known d and u.

For simulation of adhesion we use the mesh-dependent detachment criterion by Pohrt and Popov [31]. We apply Griffith' crack criterion and obtain a critical stress value p_c depending on meth-size. We compare the stress in each element with the critical value p_c and let detach those elements, whose tensile stress is larger than p_c. Based on that, a stress-based criterion for elemental separation is obtained for simulation of pull-off. This method can numerically reproduce the JKR-solution with very high accuracy. The details on the principle and numerical procedure of this method are found in reference [31].

3 Results

In simulation, the brush structure is pressed into the elastic half space by an indentation depth d and then pulled off until complete detachment under condition of controlled displacement. The results are normalized by the characteristic values of force, critical indentation in the case of a flat rigid brush structure [23],

$$\tilde{F} = \frac{F}{F_c}, \tilde{d} = \frac{d}{d_c}, \tag{11}$$

with

$$F_c = \sqrt{8\pi\varphi E^* \Delta\gamma \left(\sqrt{A_0/\pi}\right)^3}, \tag{12}$$

$$d_c = \sqrt{\frac{2\pi\varphi\Delta\gamma\left(\sqrt{A_0/\pi}\right)}{E^*}}, \tag{13}$$

where φ is the filling ratio defined as the ratio of area total cross sections of pillars, are located A_{cross}, and the nominal area A_0, $\varphi = A_{cross}/A_0$, E^* is the effective elastic modulus $E^* = E/(1-v^2)$, $\Delta\gamma$ is the work of adhesion per unit area. F_c is the adhesive force (the maximal pull-off force) in the case of the rigid flat-ended brush structure, and d_c is the critical displacement. The characteristic roughness σ and spring stiffness are normalized as

$$\tilde{\sigma} = \frac{\sigma}{d_c}, \tilde{k} = \frac{k}{E^* L}, \tag{14}$$

where L is the size of simulation area, so the nominal area $A_0 = L \times L$. The value $E^* L$ is the contact stiffness of a rigid punch with diameter L in contact with an elastic half space.

So the dimensionless stiffness indicates the stiffness of the fibril structure in comparison with the contact property.

In the present study, we used 324 pillars distributed in a square area, with the ratio $\varphi = 0.16$. In an example we show the value of the dimensionless stiffness using the values of biomaterial: pillars distributed in area $10\mu\text{m} \times 10\mu\text{m}$ have elastic modulus 1 GPa, length 2 μm and diameter 0.2 μm, and the half space has effective elastic modulus E^{*}=1 GPa. According to the beam theory pillar's stiffness is 0.02 N/mm. Contact stiffness of a rigid flat punch with this elastic half space is roughly 10 N/mm. This case corresponds to the dimensionless stiffness $\tilde{k} = 0.002$. To obtain a general law, the dimensionless stiffness $\tilde{k}$, the roughness $\tilde{\sigma}$, and the maximum indentation depth $\tilde{d}$ are varied to study their influence on adhesive strength.

3.1 Influence of roughness and preload

First, we present nine simulations of pull-off process for different roughness $\tilde{\sigma}$ ranging from 0.07 to 2.10. In all cases, the structure was first pressed up to the indentation depth corresponding to the preload $\tilde{F}_P \approx 6.5$. Spring dimensionless stiffness $\tilde{k} = 10$ means that we consider a very stiff embedding of the pillars. Dependences of normal force on indentation depth and contact area are shown in Figure 2.

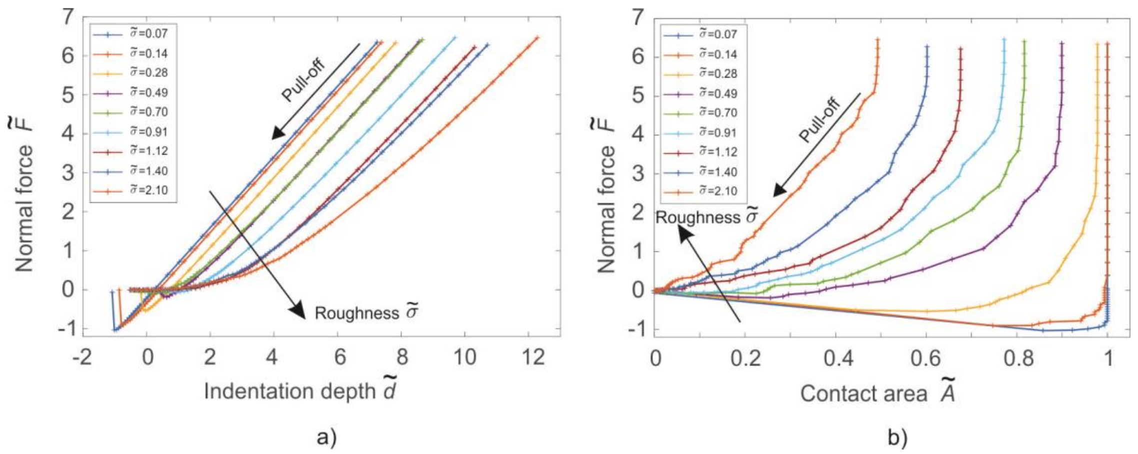

Figure 2 Dependence of normal force on indentation depth (a) and contact area (b) for different roughness. The spring stiffness is $\tilde{k} = 10$.

At the maximum indentation depth, the applied force (preload) $\tilde{F}_P$ is recorded. During the pull-off, the normal force $\tilde{F}$ changes from compression to tension. The absolute value of the minimum negative pull-off force is considered as adhesive force $\tilde{F}_A$. It is clearly seen that the adhesive force decreases with roughness. For very rough structures, there is almost no tensile force, so the adhesive force is zero. The fact that roughness reduces the strength of adhesion is a well-known fact (it is generally valid with an exception of a slight enhancement of adhesion for very small level of surface roughness [32][33][34]).

In the second series, we change the initially applied normal force $\tilde{F}_P$ (preload). This changes the preliminary contact area A achieved before reversing the force and eventually affect the adhesive force $\tilde{F}_A$. In Figure 3, the influence of preload $\tilde{F}_P$ on adhesive force $\tilde{F}_A$ is shown for different roughness $\tilde{\sigma}$. The values are averaged over 10 realizations of the rough brush structure. For a given roughness $\tilde{\sigma}$, the adhesive force $\tilde{F}_A$ increases with the preload $\tilde{F}_P$ almost linearly firstly, and ultimately reaches to a plateau where the adhesive force is preload-insensitive. This behaviour can be observed for all values of roughness, $\tilde{\sigma}$. For a very small roughness e.g. $\tilde{\sigma} = 0.070$ (blue curve in Figure 3), the structure is almost flat, so that the value of normalized adhesive force approaches one, which corresponds to a rigid flat brush structure. The quantitative analysis of roughness and preload is given in the next section together with the consideration of spring stiffness.

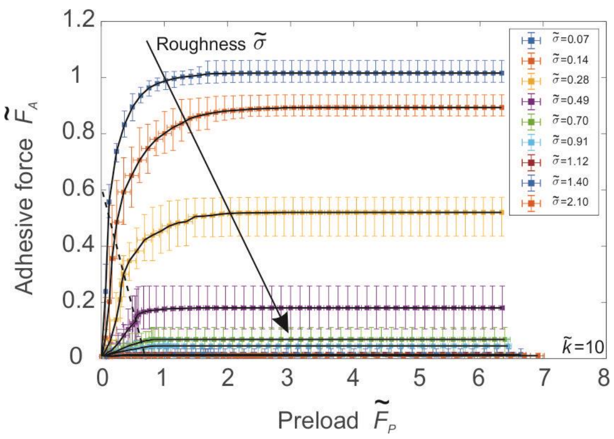

Figure 3 Dependence of the preload and the adhesive force. The spring stiffness is $\tilde{k} = 10$.

3.2 Influence of stiffness

With the same parameters as above, the simulations were repeated for different stiffness $\tilde{k}$ ranging from 10 to 0.001. The last one corresponds to very soft fibrils. The dependence of the preload and roughness on adhesive force for four selected cases $\tilde{k} = 1, 0.1, 0.01, 0.001$ are shown in Figure 4.

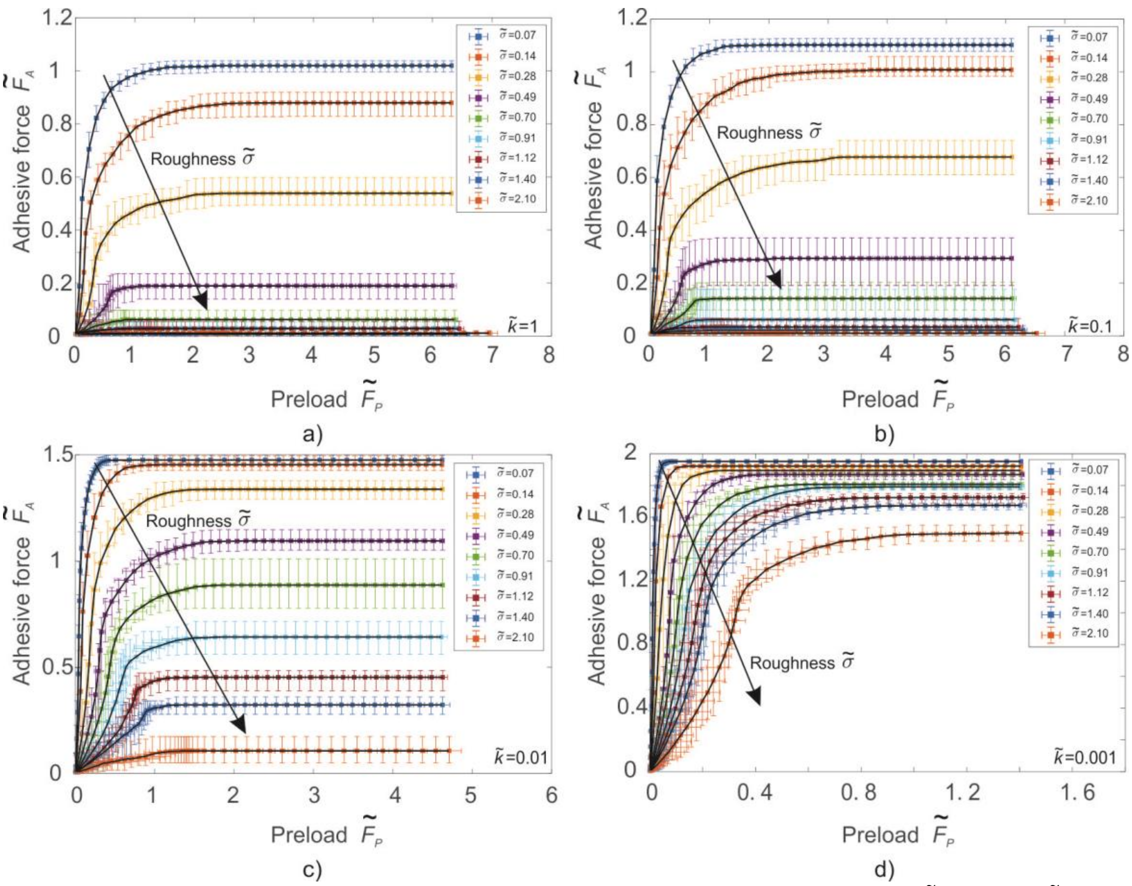

Figure 4 Dependence of adhesive force on the preload for different roughness with stiffness (a) $\tilde{k} = 1.0$; (b) $\tilde{k} = 0.1$; (c) $\tilde{k} = 0.01$; (d) $\tilde{k} = 0.001$.

With a decrease of $\tilde{k}$, the influence of roughness $\tilde{\sigma}_c$ becomes weaker, thus the adhesive force becomes "tolerant" to roughness. The case of $\tilde{k} = 1.0$ (Figure 4a) corresponds still to the quite rigid structure, and thus, the dependence is nearly the same as in the case $\tilde{k} = 10$. It is seen that the enhancement of adhesive strength is achieved when the stiffness is smaller (softer fibrils), which is especially pronounces for large roughness. For example, in the case of a quite flat and rigid structure ($\tilde{k} = 1.0$ and the smallest roughness $\tilde{\sigma} = 0.07$), the maximum adhesive force $\tilde{F}_A$ lies at 1 while it approaches 2 if the pillars are very soft with of $\tilde{k} = 0.001$ (Figure 4d). For the largest roughness $\tilde{\sigma} = 2.1$, the structure with $\tilde{k} = 1.0$ has almost vanishing adhesive strength, but with very soft pillars of $\tilde{k} = 0.001$ it remains at a very high level of $\tilde{F}_A = 1.5$.

It is noted that the ranges of *x* coordinate in four figures of Figure 4 are different. The linear stage will be smaller when reducing the stiffness of springs. Softer structure reaches to saturation stage earlier compared with stiffer one.

Let us look in more detail at the dependence of adhesive strength on preload. In the linear stage, $\tilde{F}_A$ is roughly proportional to $\tilde{F}_P$,

$$\tilde{F}_A = c\tilde{F}_P, \tag{15}$$

the slop c being known as adhesion coefficient [35][36]. In Figure 5, the dependence of the adhesion coefficient c on the roughness $\tilde{\sigma}$, (for stiffness varying between $\tilde{k} = 0.001$ and $\tilde{k} = 10$) is shown with symbols. The adhesion coefficient c decreases rapidly with roughness, especially for larger stiffness $\tilde{k}$. With increasing $\tilde{k}$, curves approach the rigid case, and they collapse practically to one curve when $\tilde{k} \geq 0.55$. For soft foundation, e.g., $\tilde{k} = 0.001$, the adhesion coefficient can reach $c = 204$ (for the smallest roughness $\tilde{\sigma} = 0.01$) which is more than 25 times larger than $c = 8$ for stiffness $\tilde{k} \geq 0.55$.

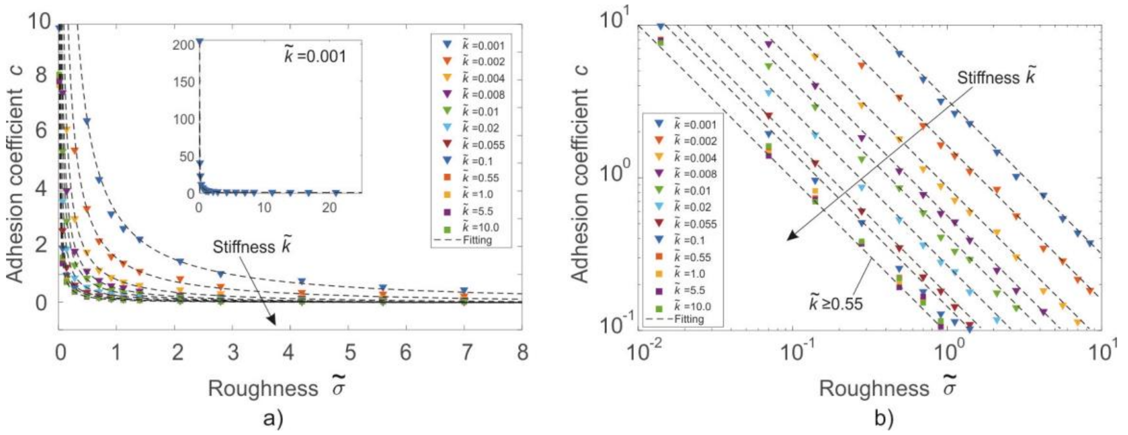

Figure 5 (a) Dependence of the adhesion coefficient on the characteristic roughness for different stiffnesses, and (b) this dependence in double logarithmic coordinates.

In [35], for elastically independent pillars where the height follows an exponential probability distribution an approximation of such a linear relation was given with $c = \frac{\tilde{F}_A}{\tilde{F}_P} = \frac{1}{\tilde{\sigma}} - 1$. Similarly, we can approximate our present results with a similar dependency

$$\tilde{F}_A = c(\tilde{\sigma}, \tilde{k}) \cdot \tilde{F}_P = \left[\alpha(\tilde{k}) \cdot \frac{1}{\tilde{\sigma}} - \beta(\tilde{k})\right] \cdot \tilde{F}_P, \tag{16}$$

where α can be interpreted as an amplification factor depending on $\tilde{k}$, comparing to the rigid brush structure, while β is the bias to determine the max roughness, after which adhesion vanishes. Fitting Eq. (12) to numerical results is shown by dashed lines in Figure 5. It is seen that the function (12) describes the relation very well. The values of α, β for different stiffness can be found in the Table 1.

For very high roughness, the adhesive force should vanish. The transition from adhering to non-adhering surfaces is rather sharp, and the critical value of roughness, $\tilde{\sigma}_c = \alpha/\beta$, can be identified with a good precision. Simulations show that this value strongly depends on the stiffness of pillars. For rigid case, the critical roughness is about 3.67. The values for other soft pillars are listed in Table 1.

Table 1 Values of α, β and $\tilde{\sigma}_c$

$\tilde{k}$	≥0.55	0.1	0.055	0.02	0.01	0.008	0.004	0.002	0.001
α	0.11	0.15	0.18	0.28	0.44	0.59	0.91	1.7	3.32
β	0.03	0.035	0.035	0.05	0.08	0.09	0.1	0.11	0.15
$\tilde{\sigma}_c$	3.67	4.29	5.14	5.6	5.5	6.56	9.1	15.45	22.13

Now we consider the region of plateau where the adhesive force is independent of preload. The dependence of adhesive force on the roughness and stiffness is shown in Figure 6.

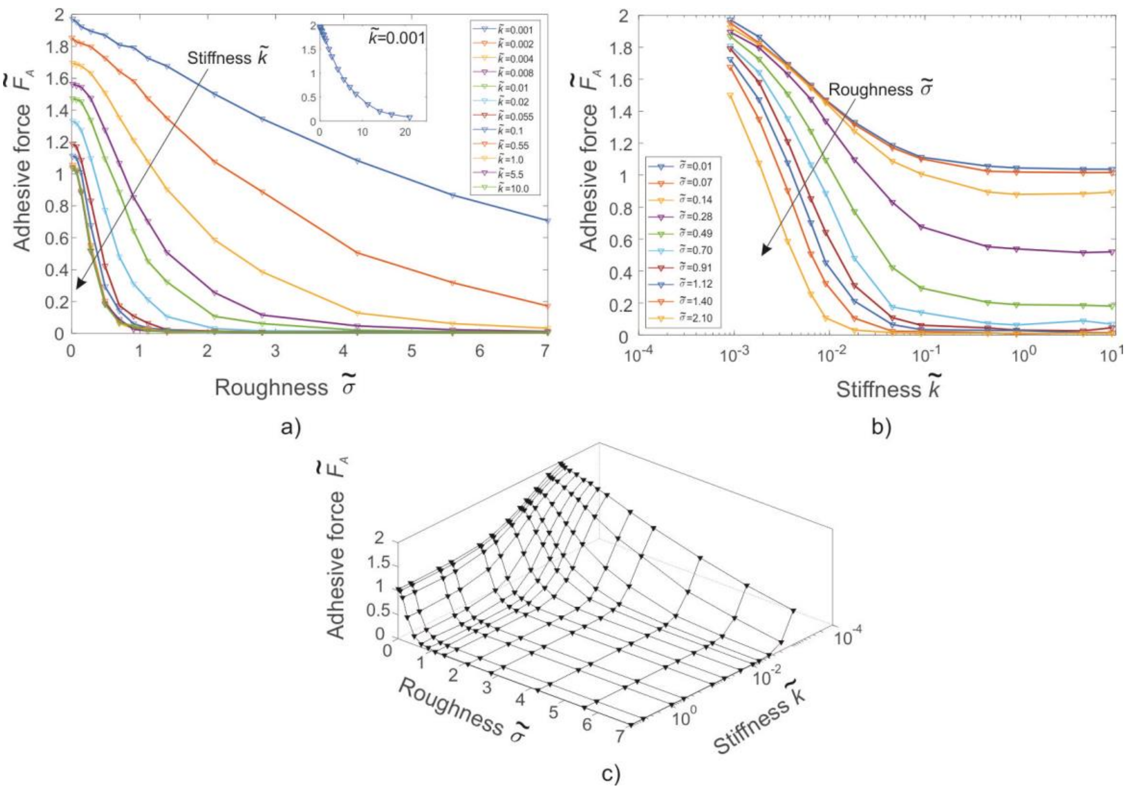

Figure 6 Dependence of adhesive force in the region of plateau on the roughness (a) and spring stiffness (b), and a three-dimensional illustration of dependence (c).

Similarly, to the linear region, the curves are approaching those in the case of rigid pillars when the stiffness is larger than 0.55, $\tilde{k} \geq 0.55$, when they all collapse to one curve. The adhesive force $\tilde{F}_A$ at the plateau decreases with roughness $\tilde{\sigma}$ and stiffness $\tilde{k}$. Similar relation between adhesive force and roughness has been numerically and experimentally obtained in other studies [5][37]. But in [5], the interaction among pillars (springs) was not considered, and it was assumed that all pillars separate at the same load and displacement individually for cases of $\tilde{\sigma} \to 0$. Figure 6 shows that decreasing pillar stiffness $\tilde{k}$ leads to the initial concept of contact splitting. In this limit (and only in this limit), the contact splitting really gives rise to a strong adhesion enhancement in comparison with the compact surface [14][38][39].

4 Conclusion

We studied the adhesive strength of a contact of a rough fibrillar structure and an elastic half space as function of stiffness of the fibrillar structure. The case of rigid pillars has been investigated recently [27]. The present model aims to bridge the limiting cases of very rigid fibrils and extremely soft fibrils (which approaches to contact splitting) [20][38][39]. We identified the relevant parameter of this transition and studied the transition in dependence of all essential material and loading parameters as preload, roughness and pillar stiffness. The stiffness of pillars was integrated into the FFT-assisted BEM directly so that the elastic interaction between pillars does not need to be considered independently.

It is known that roughness and stiffness affect the strength of adhesion significantly. Simulation results in the present work show that the adhesive force first increases approximately linearly with the preload for the weak compression, then reaches to a plateau and becomes preload-insensitive as preload increases. For a specific roughness, the maximum adhesive force in the plateau region increases with the decrease of stiffness. A critical roughness, at which adhesion vanishes, exists for every determined stiffness, and the range of this value becomes larger for smaller stiffness, i.e. softer fibrils have much better adaptability to comply larger roughness, and the detrimental effect from roughness can be compensated by decreasing stiffness. On the other side, with increasing stiffness, the maximum adhesive force as well as the adhesion coefficient will rapidly converge to that of the rigid case, especially when stiffness $\tilde{k} \geq 0.55$, all results practically collapse together. In particular, we determined the stiffness needed to make the adhesion stress "tolerant" to the roughness, and an enhancement of adhesion is obtained by decreasing stiffness.

References

[1] Autumn, K.; Peattie, A.M. Mechanisms of Adhesion in Geckos. Integrative and Comparative Biology, 2002, 42, 6, 1081–1090.

[2] Persson, B. N. J., J. On the mechanism of adhesion in biological systems. Chem. Phys., 2003, 118, 7614–7621.

[3] Arzt, E.; Gorb, S.; Spolenak, R. From micro to nano contacts in biological attachment devices. Proc. Natl. Acad. Sci. USA, 2003, 100, 10603–10606.

[4] Hui, C.-Y.; Glassmaker, N. J.; Tang, T.; Jagota, A. Design of biomimetic fibrillar interfaces: 2. Mechanics of enhanced adhesion. J. R. Soc. Interface, 2004, 135–48.

[5] Hui, C.-Y.; Glassmaker, N. J.; Jagota, A. How Compliance Compensates for Surface Roughness in Fibrillar Adhesion. The Journal of Adhesion, 2005, 81:7-8, 699-721.

[6] Porwal, P. K.; Hui, C-Y. Strength statistics of adhesive contact between a fibrillar structure and a rough substrate. J. R, Soc., Interface, 2008, 5: 441–448.

[7] Yurdumakan, B.; Raravikar, N. R.; Ajayan, P. M.; Dhinojwala, A. Synthetic gecko foot-hairs from multiwalled carbon nanotubes. Chem. Commun, 2005, 3799.

[8] Lake, G. J.; Thomas, A. G. The Strength of Highly Elastic Materials. Proc. R. Soc. Lond. A, 1967, 300, 108-119.

[9] Schargott, M. A mechanical model of biomimetic adhesive pads with tilted and hierarchical structures. Bioinspiration & biomimetics, 2009, 4 (2), 026002.

[10] Johnson, K. L.; Kendall, K.; Roberts, A. D. Surface energy and the contact of elastic solids. Proc. R. Soc. Lond. A, 1971, 324, 301–313.

[11] Kendall, K. The adhesion and surface energy of elastic solids. J. Phys. D: Appl. Phys., 1971, 4, 1186.

[12] Guidoni, G. M.; Schillo, D.; Hangen, U.; Castellanos, G.; Arzt, E.; McMeeking, R.M.; Bennewitz, R. Discrete contact mechanics of a fibrillar surface with backing layer interactions. J. Mech. Phys. Solids, 2010, 58, 1571–1581.

[13] Argatov, I.; Li, Q.; Popov, V. L. Cluster of the Kendall-type adhesive microcontacts as a simple model for load sharing in bioinspired fibrillar adhesives. Arch Appl. Mech., 2019, 89, 1447–1472.

[14] Barreau, V.; Hensel, R.; Guimard, N. K.; Ghatak, A.; McMeeking, R. M.; Arzt, E. Fibrillar elastomeric micropatterns create tunable adhesion even to rough surfaces. Adv. Funct. Mater., 2016, 26: 4687-4694.

[15] Northen, M.; Foster, K. A batch fabricated biomimetic dry adhesive. Nanotechnology, 2005, 16, 1159.

[16] Gao HJ.; Yao, HM. Shape insensitive optimal adhesion of nanoscale fibrillar structures. Proceedings of the National Academy of Sciences May 2004, 101 (21) 7851-7856.

[17] Heide-Jørgensen, S.; Budzik, M. K.; Turner, K. T. Mechanics and fracture of structured pillar interfaces. Journal of the Mechanics and Physics of Solids, 2020, 137, 103825.

[18] Morano, C.; Zavattieri, P.; Alfano, M. Tuning energy dissipation in damage tolerant bio-inspired interfaces. Journal of the Mechanics and Physics of Solids, 2020, 103965.

[19] Arzt, E.; Gorb, S.; Spolenak, R. From micro to nano contacts in biological attachment devices. Proc. Natl. Acad. Sci. USA, 2003, 100, 10603-10606.

[20] Kamperman, M.; Kroner, E.; del Campo, A.; McMeeking, R. M.; Arzt, E. Functional Adhesive Surfaces with “Gecko” Effect: The Concept of Contact Splitting. Adv. Eng. Mater., 2010, 12, 335-348.

[21] Takahashi, K., et al. Geckos’ foot hair structure and their ability to hang from rough surfaces and move quickly. Int. J. Adhesion & Adhesives, 2006, 26, 639-643.

[22] Bhushan, B. Adhesion of multi-level hierarchical attachment systems in gecko feet. Journal of Adhesion Science and Technology, 2007, 21:12-13, 1213-1258.

[23] Li, Q.; Popov, V. L. Adhesive force of flat indenters with brush-structure. Facta Univ., Ser.: Mech. Eng., 2018, 16, 1–8.

[24] He, X.; Li, Q.; Popov, V. L. Simulation of Adhesive Contact of Soft Microfibrils. Lubricants, 2020, 8, 94.

[25] Pohrt, R.; Li, Q. Complete boundary element formulation for normal and tangential contact problems. Phys. Mesomech., 2014, 17, 334–340.

[26] Popov, V. L.; Pohrt, R.; Li, Q. Strength of adhesive contacts: Influence of contact geometry and material gradients. Friction, 2017, 5, 308–325.

[27] Li, Q., Popov, V. L. Adhesive contact of rough brushes. Beilstein J. Nanotechnol., 2018, 9, 2405–2412.

[28] Boussinesq, V. J. Application des Potentiels l'Etude del'Equilibre et du. S. 1, Gautier-Villar, 1882.

[29] Popov, V. L. Adhesive contact between a rigid body of arbitrary shape and a thin elastic coating. 2018.

[30] Wang, Q.; Sun, L.; Zhang, X.; Liu, S.; Zhu D. FFT-Based Methods for Computational Contact Mechanics. Front. Mech. Eng., 2020, 6, 61.

[31] Pohrt, R.; Popov, V. L. Adhesive contact simulation of elastic solids using local mesh-dependent detachment criterion in boundary elements method. Facta Univ. Ser. Mech. Eng., 2015, 13, 3–10.

[32] Li, Q.; Pohrt, R.; Popov, V. L. Adhesive Strength of Contacts of Rough Spheres. Frontiers in Mechanical Engineering, 2019, 5, 7.

[33] Briggs, G. A. D.; Briscoe, B. J. The effect of surface topography on the adhesion of elastic solids. J. Phys. D Appl. Phys., 1977, 10, 2453–2466.

[34] Guduru, P. R. Detachment of a rigid solid from an elastic wavy surface: theory. J. Mech. Phys. Solids, 2007, 55, 445–472.

[35] Popov, V. L. Contact Mechanics and Friction. Physical Principles and Applications, 2nd ed.; Springer: Berlin, Germany, 2017.

[36] Barber, J. R. Contact Mechanics; Springer: Berlin, Germany, 2018.

[37] Fuller, K. N. G.; Tabor, D. The Effect of Surface Roughness on the Adhesion of Elastic Solids, 1975.

[38] Varenberg, M.; Murarash, B.; Kligerman, Y.; Gorb, S. N. Geometry-controlled adhesion: revisiting the contact splitting hypothesis. Appl. Phys. A: Mater. Sci. Process, 2011, 103, 933–938.

[39] Boesel, L. F.; Greiner, C.; Arzt, E.; del Campo, A. Gecko-Inspired Surfaces: A Path to Strong and Reversible Dry Adhesives. Adv. Mater., 2010, 22: 2125-2137.